

# HIGHLIGHTS OF THE LATEST STANDARD MODEL MEASUREMENTS IN ATLAS\*

YI YU

on behalf of the ATLAS Collaboration

University of Science and Technology of China, China

*Received 22 March 2024, accepted 19 June 2024,  
published online 5 August 2024*

Recent physics results from the ATLAS experiment, covering both high-precision measurements and exciting observations, are presented. These results involve the production of vector bosons, multi-jets, and top quarks. Building on top of measuring production cross sections, these results also offer determination of the Standard Model parameters, confrontation of state-of-art predictions, as well as constraints of new physics models in a model-independent way.

DOI:10.5506/APhysPolBSupp.17.5-A15

## 1. Introduction

The Large Hadron Collider (LHC) [1] provides unprecedented opportunities to probe the fundamental particles and interactions at energy and luminosity frontiers. The Standard Model (SM) of particle physics is known as an effective and non-unified theory below the Planck scale and, therefore, precision measurements of the SM at the LHC experiments are one of the most crucial means to further reveal the inner structure of the theory and seek for sign of new physics. After the discovery of the Higgs boson, more rare SM processes are observed in succession, such as vector-boson scattering, tri-boson and multi-top productions, which offers new territories that might be used to look for new physics contributions and their interferences with the SM. In addition, along with the accumulating statistics of the collision data, the impact of theoretical uncertainties in a given measurement get dominant and, therefore, a better understanding of fundamental parameters and the modelling of SM backgrounds via the measurements plays a particularly significant role now. This paper selects several latest and representative

---

\* Presented at the 30<sup>th</sup> Cracow Epiphany Conference on *Precision Physics at High Energy Colliders*, Cracow, Poland, 8–12 January, 2024.

Standard Model measurements in ATLAS [2], and focus on revealing what the best precision we have achieved, what the plausible direction is for future measurements, and how these measurements can be interpreted to benefit relevant studies of the SM and new physics. In the following, each section will discuss a dedicated topic of physics results.

## 2. Determinations of fundamental parameters of the SM

### 2.1. $m_W$ reanalysis

The  $W$ -boson mass is one of the paramount SM parameters with its dependence on  $m_Z$ ,  $\alpha$ ,  $G_\mu$ ,  $m_H$ , and gauge couplings in the electroweak theory, moreover, it can receive potential contributions from new resonances via the loop corrections. The  $pp$  collision dataset with an integrated luminosity of  $4.6 \text{ fb}^{-1}$  at  $\sqrt{s} = 7 \text{ TeV}$  is revisited to perform this measurement [3]. The reanalysis embraces improvements on the modelling of QCD effects, a powerful profile-likelihood fit technique [4], and the new, advanced CT18NNLO PDF [5]. A simultaneous fit of  $p_T^l$  and  $m_T^W$  distributions is used to measure  $m_W$ . As shown in figure 1, a  $m_W$  measured value consistent with the previous ATLAS measurement [6] is obtained, with an uncertainty reduced by 15%. No deviation from the SM expectation is observed.

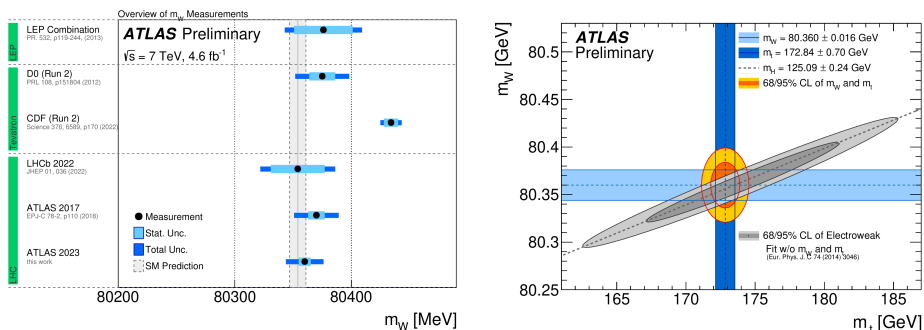


Fig. 1. Left: The measured value of  $m_W$  is compared to SM prediction from the global electroweak fit, and to the combined values of  $m_W$  measured at LEP, Tevatron, and the LHC. Right: The 68% and 95% confidence-level contours of the  $m_W$  and  $m_t$  indirect determinations from the global electroweak fit are compared to the 68% and 95% confidence-level contours of the ATLAS measurements of the top-quark and  $W$ -boson masses. From Ref. [3].

### 2.2. $\alpha_s$ extraction from $p_T^Z$

The recoil of the  $Z$  boson is sensitive to quark and gluon emissions and can be used to determine the strong coupling constant in the Sudakov peak

region. The extraction [7] is based on the ultra-high precise double differential cross-section measurement [8], which was performed as a function of  $Z$ -boson transverse momentum and rapidity, by using the  $pp$  collision data corresponding to an integrated luminosity of  $20.2 \text{ fb}^{-1}$  at the center-of-mass energy of 8 TeV. The predictions are evaluated at the third order of  $\alpha_s$  in the perturbative QCD theory, supplemented by the resummation of logarithmically enhanced contributions in the low transverse-momentum region of the lepton pairs ( $N^4\text{LLa} + N^3\text{LO}$ ) [9] using a  $N^3\text{LO}$  MSHT20 [10] as the baseline PDF set. In addition, the low- $p_T^Z$  region was excluded in previous PDF fits, largely avoiding the issue arising from the correlation between this extraction and the simultaneously determined PDFs and  $\alpha_s$  used in the predictions. As shown in figure 2, the strong-coupling constant at the reference scale corresponding to the  $Z$ -boson mass is found to be  $\alpha_s(m_Z) = 0.1183 \pm 0.0009$ , which is compatible with other determinations and with the world-average

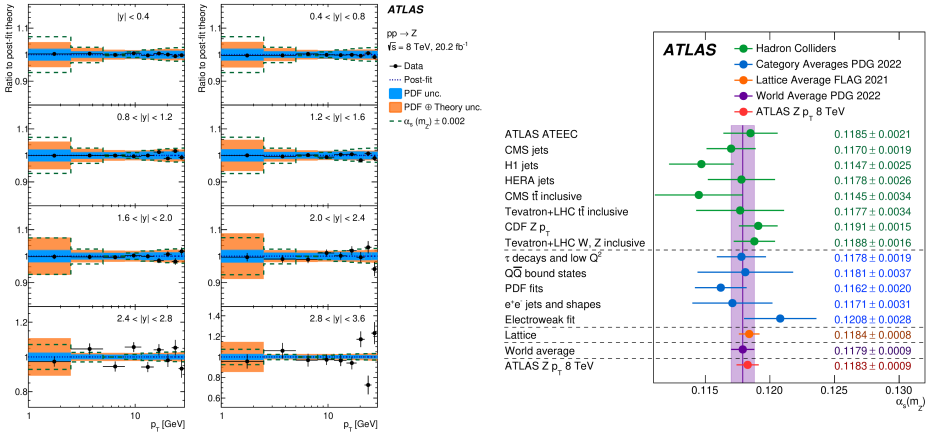


Fig. 2. (Colour on-line) Left: Ratios of the measured double-differential cross sections to the post-fit predictions, both as functions of the transverse momentum and rapidity of the  $Z$  boson. The blue/grey inner band shows the PDF uncertainties of the predictions pulled and constrained by the fit, and the orange/light grey band shows the PDF and all other unconstrained theoretical uncertainties added in quadrature. The measured cross sections are corrected by the post-fit pull of the luminosity uncertainty. The vertical error bars show the experimental uncertainties of the measurement. The dashed lines show post-fit predictions in which  $\alpha_s(m_Z)$  is varied by  $\pm 0.002$  and all other parameters are kept fixed. Right: Comparison of the determination of  $\alpha_s(m_Z)$  from the  $Z$ -boson transverse-momentum distribution (ATLAS  $Z p_T$  8 TeV) with other determinations at hadron colliders, with the PDG category averages, with the lattice QCD determination, and with the PDG world average. From Ref. [7].

values. Due to the benefit from the significant sensitivity given by  $p_T^Z$  and the high accuracy of the state-of-the-art theory predictions, this work gives the most precise experimental determination of  $\alpha_s(m_Z)$  achieved so far.

### 2.3. $\alpha_s$ extraction from TEEC

Large momentum transfer in the multi-jets production provides an ideal testing ground for the perturbative QCD theory, with the event shapes reconstructed from final-state particles characterizing the hadronic energy flow in the collisions. Measurements of transverse energy–energy correlations [11] and their associated azimuthal asymmetries in multi-jet events are presented in bins of the scalar sum of the transverse momenta of the two leading jets using a data sample corresponding to  $139 \text{ fb}^{-1}$  of proton–proton collisions at the center-of-mass energy of 13 TeV [12]. In figure 3, they are compared to next-to-next-to-leading-order perturbative QCD calculations [13, 14] for the first time, and found to be in good agreement. A simultaneous fit to all transverse energy–energy correlation distributions across different kinematic regions yields a value of  $\alpha_s(m_Z) = 0.1175 \pm 0.0006(\text{exp.})_{-0.0017}^{+0.0034}(\text{theo.})$ , while the global fit to the asymmetry distributions yield  $\alpha_s(m_Z) = 0.1185 \pm 0.0009(\text{exp.})_{-0.0012}^{+0.0025}(\text{theo.})$ .

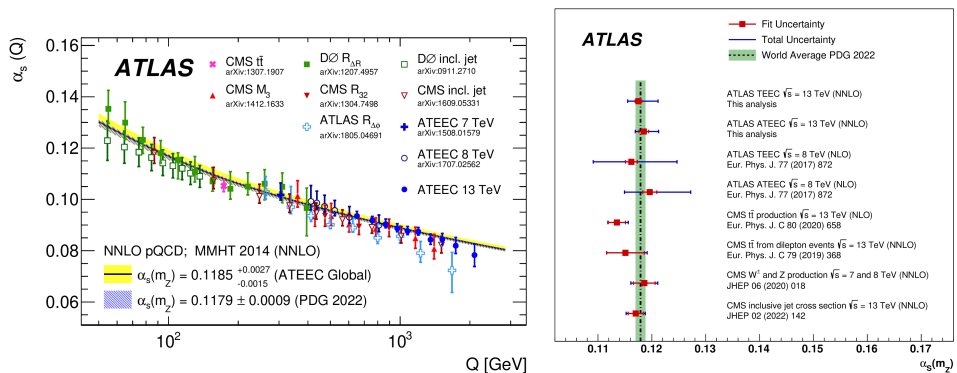


Fig. 3. Left: Comparison of the values of  $\alpha_s(Q)$  determined from fits to the ATEEC functions with the QCD prediction using the world average as input (hatched band) and the value obtained from the global fit (solid band). Results from previous analyses, both from ATLAS and from other experiments, are also included, showing excellent agreement with the current measurements and with the world average. The value of  $Q$  for the TEEC 13 TeV points is chosen as half of the average of  $\hat{H}_T$  in each  $H_{T2}$  bin. Right: Comparison of the values of  $\alpha_s(m_Z)$  determined from different analyses by ATLAS and CMS. From Ref. [12].

2.4.  $Z$  boson invisible decay width

A measurement of the  $Z \rightarrow \nu\nu + \text{jets}$  to  $Z \rightarrow \ell\ell + \text{jets}$  differential cross-section ratio as a function of the  $Z$ -boson transverse momentum is performed with  $37 \text{ fb}^{-1}$  of 13 TeV proton–proton data recorded by ATLAS in 2015 and 2016, in which events are required to contain exactly one energetic jet with  $p_{\text{T}} > 110 \text{ GeV}$  to ensure a common phase space in the ratio calculation [15]. After the bin-wise corrections for detector effects, FSR and  $\gamma^*$  contributions, the invisible width of the  $Z$  boson is determined via a constant  $\chi^2$  fit of  $R^{\text{miss}}(p_{\text{T},Z})$  with the measured leptonic width [16, 17] as the prior input

$$\begin{aligned}
 R^{\text{miss}}(p_{\text{T},Z}) &\equiv \left( \frac{d\sigma(Z(\rightarrow \text{inv}) + \text{jets})}{dp_{\text{T},Z}} \right) / \left( \frac{d\sigma(Z(\rightarrow \ell\ell) + \text{jets})}{dp_{\text{T},Z}} \right) \\
 &= \left( \frac{d\sigma(Z + \text{jets}) \times \text{BR}(Z \rightarrow \text{inv})}{dp_{\text{T},Z}} \right) / \left( \frac{d\sigma(Z + \text{jets}) \times \text{BR}(Z \rightarrow \ell\ell)}{dp_{\text{T},Z}} \right). \quad (1)
 \end{aligned}$$

The obtained value of  $506 \pm 2(\text{stat.}) \pm 12(\text{syst.}) \text{ MeV}$  is the most precise experimental result for recoil-based final states to date. As shown in figure 4, the result is in agreement with other recoil-based measurements, with the most precise determination of  $\Gamma(Z \rightarrow \text{inv})$  from LEP [16], and with the Standard Model prediction based on three neutrino generations [17].

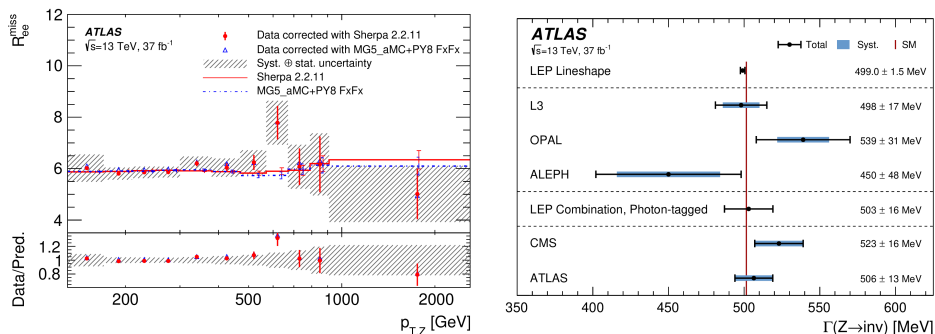


Fig. 4. (Colour on-line) Left: Measured  $R^{\text{miss}}$  of electrons as a function of  $p_{\text{T},Z}$  in the corrected phase space. The error bars on the measured red/grey points show the statistical uncertainty and the grey hashed bands show the combined statistical and systematic uncertainties. For both of the predictions, statistical uncertainties and uncertainties due to the  $\gamma^*$  correction are shown by the vertical bars. Right:  $\Gamma(Z \rightarrow \text{inv})$  measured in this paper and by the LEP experiments L3, OPAL, ALEPH and the photon-tagged combination and by the CMS experiment. The total uncertainties are represented by the black error bars and the systematic uncertainty as the blue/light grey bands. The LEP combination of the photon-tagged results and the result from the lineshape measurements only quote their total uncertainty. The Standard Model prediction is shown by the solid vertical red/grey line. From Ref. [15].

### 3. Precision measurements of gauge boson processes

#### 3.1. $p_T^V$ measurements

The non-zero  $p_T^V$  arises from higher-order corrections and non-perturbative effects, and the cross section in the Sudakov peak region [18] ( $p_T^V < 30$  GeV) is difficult to model accurately with the pQCD calculations, with more complex resummation formalisms and calculations required to cancel out the divergence resulting from the soft and collinear emissions. Another possibility is to use parton shower programs that evolve parton fragmentation through the DGLAP formalism. The precise measurement of  $p_T^V$  is of paramount importance, because that can enable discrimination between the various physics models and contribute to the tuning effectively, which leads to great precision in modelling the vector-boson process and set a foundation for ultra-high electroweak measurements.

As the resolution of the hadronic recoil drastically decreases in high pile-up experimental conditions, the measurements of the transverse momentum of the  $W$  and  $Z$  bosons are performed at 5 and 13 TeV from dedicated LHC runs with the reduced instantaneous luminosity, which are then compared to various MC predictions [19] in figures 5 and 6, and discussed below.

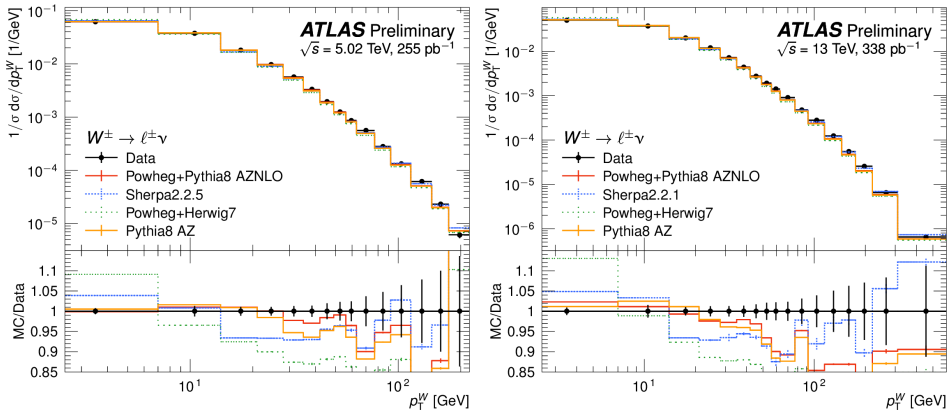


Fig. 5. (Colour on-line) Measurements of normalized differential distributions for  $W^\pm$  at 5 TeV (left) and 13 TeV (right) compared to a variety MC predictions of multijet-merged NLO Sherpa [20] and MadGraph FxFx+Pythia8 [21] samples (coloured lines). The lower panels show the ratio of prediction to data with data markers centred at 1 and error bars giving the size of the total measurement uncertainties. From Ref. [19].

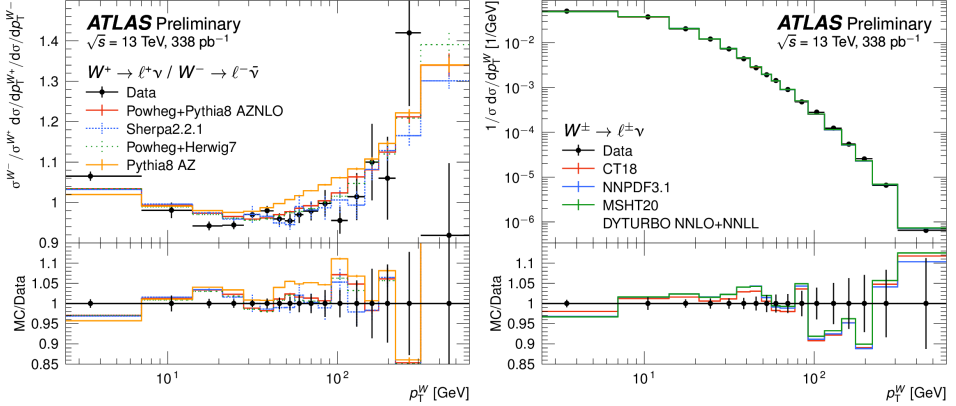


Fig. 6. (Colour on-line) Left: Measurements of normalized differential distributions at 13 TeV (black points) for the ratio of  $W^+$  and  $W^-$  compared to a variety of MC predictions (coloured lines). Right: Measurements of normalised differential distributions at 13 TeV for  $W^\pm$  compared to DYTURBO MC predictions with different PDF sets (coloured lines). The lower panels show the ratio of prediction to data with data markers centred at one and error bars giving the size of the total measurement uncertainties. From Ref. [19].

Parton shower MC predictions show significant differences, which are largely common to  $W^+$ ,  $W^-$ , and  $Z$  productions, hence, the ratio of cross sections are in relatively better agreement. The better agreement is visible at  $\sqrt{s} = 5.02$  TeV, especially for predictions tuned to  $Z$ -production data at  $\sqrt{s} = 7$  TeV. Currently the higher-order, resummed predictions from DYTURBO (NNLO+NNLL) match the data best across the spectra.

### 3.2. Double differential cross sections in $Z$ boson $p_T$ and $Y$

A first-time extraordinarily precise double-differential measurement of the  $Z$  boson in the full phase space of the decay leptons is performed with the dataset corresponding to an integrated luminosity of 20.2 fb<sup>-1</sup> at the centre-of-mass energy of 8 TeV, through a four-dimensional lepton angular distribution as a function of  $p_T^l$  and  $y^l$  within the  $Z$ -pole region,  $80 < m^l < 100$  GeV, and within the range of  $|y^l| < 3.6$  [8].

Such a 4D-measurement is achieved via a profile likelihood fit, extracting simultaneously the eight angular coefficients [22, 23] and the corresponding unpolarized cross section as parameters of interest in each measurement bin in the  $(p_T, |y|)$  space.

In figure 7, the results for the rapidity-dependent transverse momentum distributions are compared to several state-of-the-art predictions at third-order accuracy in the perturbative QCD, supplemented by approxi-

mate  $N^4\text{LL } q_T$  resummation of logarithmically-enhanced contributions. The total uncertainty of the normalized cross-section measurements in the peak region of the  $p_T$  distribution is dominated by statistical uncertainties, and increases as a function of rapidity from 0.5–1.0% for  $|y| < 2.0$  to 2–7% at higher rapidities, with experimental and theoretical systematics at the few per mille level over most of the range. The data and predictions are in good agreement within 5%.

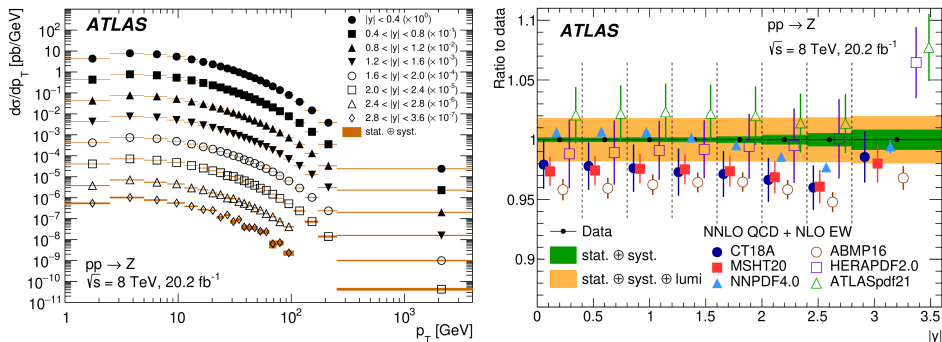


Fig. 7. Left: Measured absolute differential  $d\sigma/dp_T$  cross sections with their total uncertainties shown as a function of  $p_T$  for each  $|y|$  bin. The uncertainty of 1.8% in the integrated luminosity is not included. Right: Ratio comparison between the  $d\sigma/dy$  measurements and NNLO QCD predictions obtained from DYTURBO using different NNLO PDF sets. The uncertainty bands in the predictions only show the uncertainties specific to each PDF set (the uncertainties from CT18A have been rescaled from 95% to 68% confidence level). From Ref. [8].

The differential rapidity distributions integrated over  $p_T$  are more precise, with accuracies from 0.2–0.3% for  $|y| < 2.0$  to 0.4–0.9% at higher rapidities and are compared to fixed-order QCD predictions using the most recent parton distribution functions that display a varying degree of agreement with the data.

The total  $Z/\gamma^* \rightarrow ll$  production cross section in the  $Z$  pole region ( $|y| < 3.6$ ) is measured as  $\sigma_Z = 1055.3 \pm 0.7(\text{stat.}) \pm 2.2(\text{syst.}) \pm 19.0(\text{lumi.})$  pb.

### 3.3. The same-sign $W$ -boson pair measurement

With the  $139 \text{ fb}^{-1}$  of proton–proton collision data recorded by ATLAS at  $\sqrt{s} = 13 \text{ TeV}$ , the measurement of fiducial and differential cross sections for both the inclusive and electroweak production of the same-sign  $W$ -boson pair in association with two jets are performed by selecting two the same-charge leptons, electron or muon, and at least two jets with large invariant mass and a large rapidity difference [24]. As shown in figure 8, the measured

fiducial cross sections for electroweak and inclusive  $W^\pm W^\pm jj$  production are  $2.92 \pm 0.22(\text{stat.}) \pm 0.19(\text{syst.})$  fb and  $3.38 \pm 0.22(\text{stat.}) \pm 0.19(\text{syst.})$  fb, respectively, in agreement with the Standard Model predictions. However, several large mis-modellings are visible in the middle- $m_T$  and the low- $m_{jj}$  regions, which can be found in figure 9. The measurements are further used to constrain anomalous quartic gauge couplings by extracting 95% confidence level intervals on dimension-8 operators predicted in the Eboli model [25]. A search for doubly-charged Higgs bosons [26] is also conducted via the vector-boson fusion processes, in which the largest deviation from the Standard Model occurs for an  $H^{\pm\pm}$  mass near 450 GeV, with a global significance of 2.5 standard deviation.

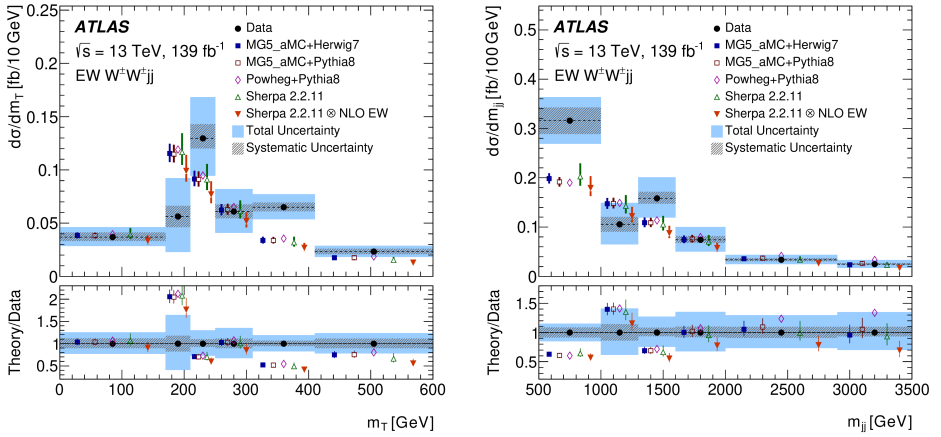


Fig. 8. Fiducial differential cross sections for the EW  $W^\pm W^\pm jj$  production as a function of (left)  $m_T$  and (right)  $m_{jj}$ . The measured data are shown as black points with horizontal bars indicating the bin range and hatched (filled) boxes representing the systematic (total) uncertainty. Different SM predictions as described in the text are compared to the data. The vertical error bars shown on the predictions correspond to the uncertainty coming from the variations of the renormalisation and factorisation scales, PDF and  $\alpha_s$ . Overflow events are included in the last bin. The lower panel of each plot shows the ratio of the predicted to measured cross sections. From Ref. [24].

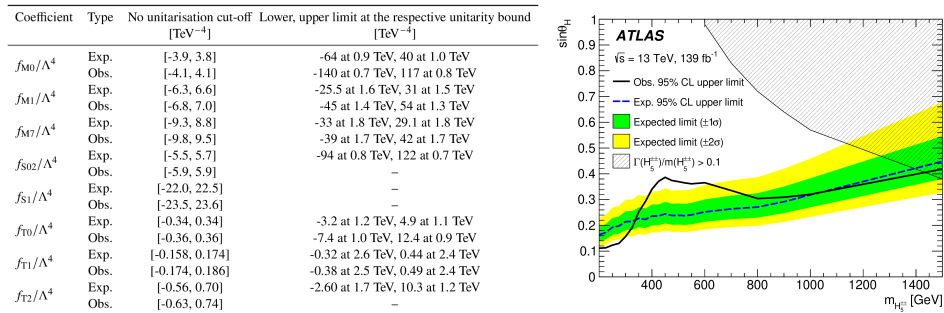


Fig. 9. (Colour on-line) Left: Expected and observed limits on the Wilson coefficients for various operators without any unitarisation procedure and with a unitarisation cut-off at the unitarity bound. The last column represents lower and upper limits at the respective cut-off value, where the unitarity bound and experimental bound cross. Cases where no crossing with the unitarity bound was found in the scanned region above 600 GeV are labelled “-”. The notation S02 is used to indicate that the coefficients corresponding to the operators  $O_{S0}$  and  $O_{S2}$  are assigned the same value. The limits on M7 are obtained without taking into account the SM-EFT interference for the EW  $WZjj$  final state. Right: Expected and observed exclusion limits at 95% C.L. for  $\sin\theta_H$  as a function of  $m_{H_5^{\pm\pm}}$  in the GM model. The green/grey (yellow/light grey) band is the 68% (95) confidence interval around the median expected limit. The exclusion limits for  $\sin\theta_H$  are shown up to  $m_{H_5^{\pm\pm}} = 1500$  GeV given the low sensitivity in the GM model above that mass. The hatched region covers the parameter space where the intrinsic width of the  $H^{++}$  boson would be larger than 10 of the mass and is disfavoured in the GM model. From Ref. [24].

## 4. Observations of top productions

### 4.1. Four-top production

The observation of  $t\bar{t}t\bar{t}$  production using 140 fb<sup>-1</sup> of data at  $\sqrt{s} = 13$  TeV is presented via a reanalysis with various improvements, including the lower- $p_T$  requirement on lepton and jets, better object definition and background modelling [27]. Additionally, the normalization of the  $t\bar{t}W$  background in jet multiplicity bins is determined using a data-driven approach, and a Graph Neural Network is further used to separate the  $t\bar{t}t\bar{t}$  signal from the background. The observed (expected) significance of the measured  $t\bar{t}t\bar{t}$  signal with respect to the SM background-only hypothesis is 6.1 (4.3) standard deviations. The measured production cross section is  $\sigma_{t\bar{t}t\bar{t}} = 22.5_{-4.3}^{+4.7}(\text{stat.})_{-3.4}^{+4.6}(\text{syst.})$  fb, which is consistent with the SM predictions within around 1.8 standard deviations and with the previous ATLAS measurement.

### 4.2. Quantum entanglement in $t\bar{t}$

The spin correlation between the top quark and anti-top quark is used to probe the effects of quantum entanglement, in proton–proton collision events with an integrated luminosity of  $140 \text{ fb}^{-1}$  at the center-of-mass energy of 13 TeV [28], by defining an experimental entanglement observable as  $D = -3 \langle \cos \phi \rangle$  [29], where  $\langle \cos \phi \rangle$  is the average value of the cosine of the angle (dot product) between the charged-lepton in their parent top- and anti-top-quark rest frames. The existence of an entangled state is demonstrated if the measurement satisfies  $D < -1/3$ .

The entanglement marker is found to be  $D = -0.547 \pm 0.002(\text{stat.}) \pm 0.021(\text{syst.})$  for  $340 < m_{t\bar{t}} < 380 \text{ GeV}$ . As shown in figure 10, the observed result is more than five standard deviations away from a scenario without entanglement and hence leads to both the first observation of entanglement in a pair of quarks and the highest energy observation of entanglement to date.

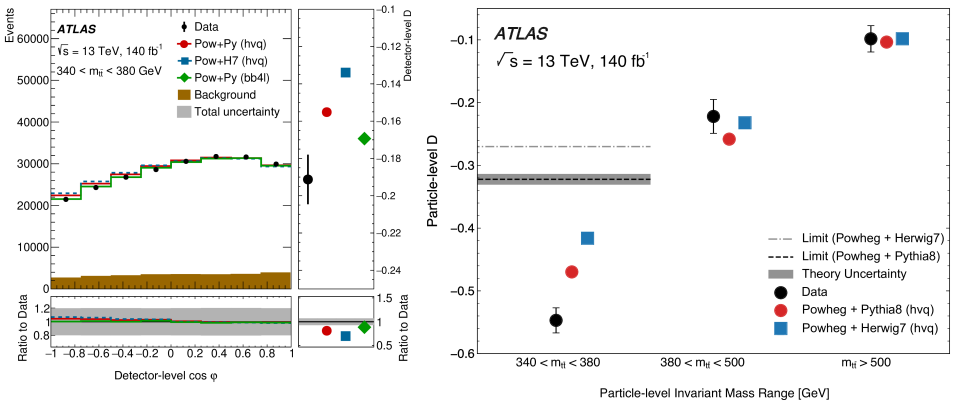


Fig. 10. Left: The left panel shows the  $\cos \phi$  observable in the signal region at the detector level and the right panel shows the entanglement marker  $D$ , calculated from the detector-level distributions, from three different MC generators; distributions are shown after background processes are subtracted. The uncertainty band shows the uncertainties from all sources added in quadrature. Right: The particle-level  $D$  results in the signal and validation regions compared with various MC models. The entanglement limit shown is a conversion from its parton-level value of  $D = -1/3$  to the corresponding value at the particle level, and the uncertainties which are considered for the band are described in the text. From Ref. [28].

## 5. Conclusion

Precision measurements are crucial probes to the Standard Model at the LHC. Confronting with the state-of-art pQCD calculations and parton-shower-based MC predictions can help improve modelling precision of physics processes and lead to a reduction of theoretical uncertainties, which generally benefits any physics studies at the frontiers. Moreover, any anomaly in the fundamental parameters of SM would be a sign of new physics, and similarly, the model-independent searches via the interpretation in effective field theories are common means of indirect search for new physics. Extensive precise measurements in ATLAS are presented with highlights of multiple measurements in the Drell–Yan processes that reach the few percent to per-mille level precision compared with NN(N)LO QCD predictions. Besides that, the diboson processes are seen as the favourable laboratory to study electroweak symmetry breaking and probes to heavy resonances and EFTs, especially for the less constrained dimension-8 operators by the LEP experiment. The 4-top process, sensitive to the top-quark Yukawa coupling, is also observed and can be used to constrain the Higgs oblique parameter and other new physics effects. Finally, the quantum entanglement measurement of top quarks paves the way to use high-energy colliders as a laboratory to study quantum information and foundational problems in quantum mechanics, which is of particular interest due to their relativistic nature, and the richness of the interactions and symmetries that can be probed there.

Copyright 2024 CERN for the benefit of the ATLAS Collaboration.  
CC-BY-4.0 license.

## REFERENCES

- [1] L. Evans, P. Bryant, *J. Instrum.* **3**, S08001 (2008).
- [2] ATLAS Collaboration (G. Aad *et al.*), *J. Instrum.* **3**, S08003 (2008).
- [3] ATLAS Collaboration, «Improved  $W$  boson Mass Measurement using 7 TeV Proton–Proton Collisions with the ATLAS Detector», ATLAS-CONF-2023-004, <https://cds.cern.ch/record/2853290>
- [4] G. Cowan, K. Cranmer, E. Gross, O. Vitells, *Eur. Phys. J. C* **73**, 2501 (2013).
- [5] T.J. Hou *et al.*, *Phys. Rev. D* **103**, 014013 (2021).
- [6] ATLAS Collaboration (M. Aaboud *et al.*), *Eur. Phys. J. C* **78**, 110 (2018).
- [7] ATLAS Collaboration, [arXiv:2309.12986](https://arxiv.org/abs/2309.12986) [hep-ex], submitted to *Nat. Phys.*

- [8] ATLAS Collaboration (G. Aad *et al.*), *Eur. Phys. J. C* **84**, 315 (2024), [arXiv:2309.09318 \[hep-ex\]](#).
- [9] S. Camarda, L. Cieri, G. Ferrera, *Phys. Rev. D* **104**, L111503 (2021).
- [10] S. Bailey *et al.*, *Eur. Phys. J. C* **81**, 341 (2021).
- [11] G. Altarelli, «The Development of Perturbative QCD», *World Scientific*, 1994.
- [12] ATLAS Collaboration (G. Aad *et al.*), *J. High Energy Phys.* **2023**, 85 (2023).
- [13] M. Czakon, A. Mitov, R. Poncelet, *Phys. Rev. Lett.* **127**, 152001 (2021); *Erratum ibid.* **129**, 119901 (2022).
- [14] M. Alvarez *et al.*, *J. High Energy Phys.* **2023**, 129 (2023).
- [15] ATLAS Collaboration, *Phys. Lett. B* **854**, 138705 (2024), [arXiv:2312.02789 \[hep-ex\]](#).
- [16] ALEPH, DELPHI, L3, OPAL, SLD collaborations, LEP Electroweak Working Group, SLD Electroweak and Heavy Flavour Groups, *Phys. Rep.* **427**, 257 (2006).
- [17] Particle Data Group (R.L. Workman *et al.*), *Prog. Theor. Exp. Phys.* **2022**, 083C01 (2022).
- [18] V.V. Sudakov, *Sov. Phys. JETP* **3**, 65 (1956).
- [19] ATLAS Collaboration, «Precise measurements of  $W$  and  $Z$  transverse momentum spectra with the ATLAS detector at  $\sqrt{s} = 5.02$  TeV and 13 TeV», ATLAS-CONF-2023-028, <https://cds.cern.ch/record/2861057>
- [20] J. Alwall *et al.*, *J. High Energy Phys.* **2014**, 079 (2014).
- [21] R. Frederix, S. Frixione, *J. High Energy Phys.* **2012**, 061 (2012).
- [22] E. Mirkes, *Nucl. Phys. B* **387**, 3 (1992).
- [23] A. Mishra, J. Reinhardt, H. Stocker, W. Greiner, *Phys. Rev. C* **66**, 064902 (2002).
- [24] ATLAS Collaboration (G. Aad *et al.*), *J. High Energy Phys.* **2024**, 26 (2024), [arXiv:2312.00420 \[hep-ex\]](#).
- [25] O.J.P. Éboli, M.C. Gonzalez-Garcia, J.K. Mizukoshi, *Phys. Rev. D* **74**, 073005 (2006).
- [26] H. Georgi, M. Machacek, *Nucl. Phys. B* **262**, 463 (1985).
- [27] ATLAS Collaboration (G. Aad *et al.*), *Eur. Phys. J. C* **83**, 496 (2023).
- [28] ATLAS Collaboration, [arXiv:2311.07288 \[hep-ex\]](#), submitted to *Nature*.
- [29] Y. Afik, J.R.M. de Nova, *Eur. Phys. J. Plus* **136**, 907 (2021).